Laser-Heated Pedestal Growth of Chromium-Doped Yttrium Aluminum Garnet Single-Crystal Fiber

C. L. Chang[1], S. L. Huang[1,2], C. Y. Lo[3], C. W. Lan[4], W. H. Cheng[5] and P. Y. Chen[6*]
[1]Institute of Photonics and Optoelectronics, National Taiwan University, Taipei 10617, Taiwan
[2]Department of Electrical Engineering, National Taiwan University, Taipei 10617, Taiwan
[3]Insitute of Optoelectronic Sciences, National Taiwan Ocean University, Keelung 20224, Taiwan
[4]Department of Chemical Engineering, National Taiwan University, Taipei 10617, Taiwan
[5]Department of Photonics, National Sun Yat-sen University, Kaoshiung 80424, Taiwan
[6]Department of Gemology, Meiho University, Pingtung 91202, Taiwan
* x00008415@meiho.edu.tw, NSC-99-2120-M-002-014-MY1

Abstract --- *The laser-heated pedestal growth (LHPG) of chromium-doped yttrium aluminum garnet (Cr:YAG) single-crystal fibers in <111> direction was investigated via a two-dimensional (2D) simulation verified by observations on the interface shapes. The normalized radial dopant profiles at the growth front are consistent with that of the grown crystal fibers in ex-situ measurements. The concentration level and distribution with the corresponding fluid flow and heat transfer were reported to visualize the phenomena that cannot be observed easily. It is viable to adjust the air/melt interface, the mass-flow distribution, and especially the growth front to acquire a crystal fiber with a desirable radial dopant distribution.*

Keywords: *Laser-heated pedestal growth, single crystal growth, Cr:YAG.*

INTRODUCTION

Single-crystal fibers are recognized for their remarkable characteristics, such as low defect density, long mode confinement, and good laser efficiency. These advantages enable their applications in passive devices [1], active devices [2], and nonlinear fiber devices [3]. For various kinds of the grown active crystal fibers to be high quality devices, the concentration level and distribution of dopant ions in the melt, especially at the growth front, are necessary to be designed and optimized in detail. However, the manipulation of parametric space and the system diagnostics are getting critical for the growth of crystal fiber, an comprehensive and quantitative information is necessary to be acquired both in experiments and simulations, especially some intermediate behaviors during the growth near the zone boundaries. Our 2D numerical model to understand the LHPG technique for growing single-crystal fibers has been achieved and verified by the experimental observations on the steady-state zone shapes [4]. Moreover, heat transfer and fluid flow in the melt, which cannot be easily diagnosed precisely, were also revealed [5].

In this paper, we report the concentration level and distribution in Cr:YAG crystal using a LHPG method [6]. The radial concentration profiles at the growth front are verified by *ex-situ* measurements with similar conditions. Compared with the corresponding fluid flow and temperature distribution, the influence of the reduction ratios on the concentration distribution, and the variation of dopant distribution by adjusting diffusion coefficient and surface-tension-temperature coefficient are analyzed.

MATHEMATICAL FORMULATION

For the consideration of dopant concentration, mass-balance equation [7] is added as fourth governing equation below:

$$\frac{\partial}{\partial r}\left(\frac{C_m}{\rho_m}\frac{\partial \psi}{\partial z}\right)-\frac{\partial}{\partial z}\left(\frac{C_m}{\rho_m}\frac{\partial \psi}{\partial r}\right)+\frac{\partial}{\partial z}\left(rD\frac{\partial C_m}{\partial z}\right)+\frac{\partial}{\partial r}\left(rD\frac{\partial C_m}{\partial r}\right)=0. \quad (1)$$

where ψ, C_m, ρ_m, D, r, and z are the stream function, dopant concentration of the melt, density of melt, diffusion coefficient of dopant ions in the melt ($cm^2 \cdot s^{-1}$), radial and axial position, respectively.

Several boundary conditions of concentration are included as follows [7]: (a) along the z-axis: $\partial C/\partial r = 0$. (b) at the growth front: $D\left(\vec{n}_g \cdot \nabla C_m\right) = U_c\left(C_m - KC_m\right)\vec{n}_g \cdot \vec{e}_z$. with $T = T_m + mC_m$ (c) At the feed front: $D\left(\vec{n}_f \cdot \nabla C_m\right) = U_s\left(C_m - C_s\right)\vec{n}_f \cdot \vec{e}_z$. with $T = T_m + mC_m$ where $\vec{n}_{f,g}$ is the unit normal vector at the feed or growth front toward the melt, $K = C_c/C_m$ is the segregation coefficient according to the phase diagram, $C_{s,c}$ is the dopant concentration of source rod or crystal fiber, $\vec{e}_z$ is the unit vector along the z axis, m is the slope of the liquids line in the phase diagram, and T_m is the melting temperature. The diffusion in the crystal is neglected comparing to that in the melt. (d) At the air/melt interface, $\vec{n}_m \cdot \nabla C = 0$. where $\vec{n}_m$ is the unit normal vector at the air/melt surface. At steady state, the average dopant concentration of the crystal fiber at the growth front is the same as that of source rod and is K times higher than that of the melt.

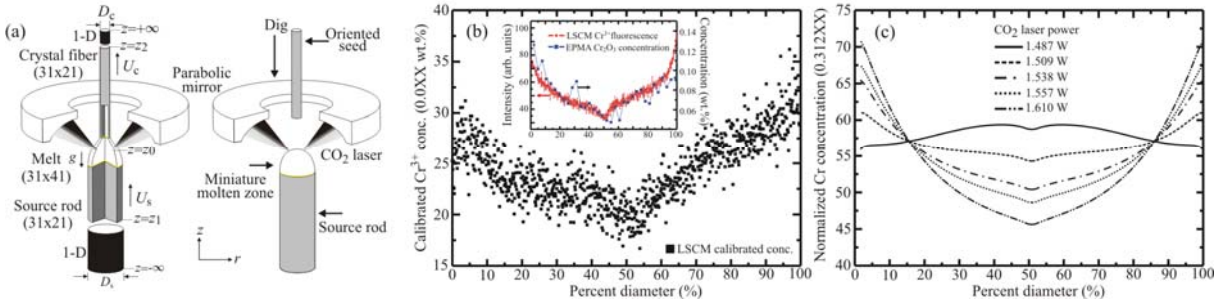

Figure 1. (a)The schematic illustration of LHPG method for growing single-crystal fibers. (b) The calibrated concentration of Cr^{3+} ions across the fiber cross sections for D_c =66 μm with the reduction ratio of 22%. The inset is the comparison and calibration between the Cr^{3+} fluorescent intensity profile measured by LSCM and the concentration of Cr_2O_3 measured by EPMA. (c) The normalized radial concentration profiles of Cr ions at the growth front at various allowable powers for the reduction ratios of 35% while K=3.2, D=10^{-2} $cm^2 \cdot s^{-1}$ and $\partial\gamma/\partial T$ =-3.5×10^{-2} $dyn \cdot cm^{-1} \cdot K^{-1}$. g, $U_{s,c}$, and $D_{s,c}$ are gravitational acceleration, drawing speed, and fiber diameters.

RESULTS AND DISCUSSION

Figure 1(a) shows the schematic illustration of LHPG method for growing single-crystal fibers [4]. The ring-shaped CO_2 laser beam was tightly focused by a parabolic mirror to melt the source rod as the pedestal and the seed rod in <111> direction was then dipped into it to form a highly-heat-concentrated miniature melt bridge. The crystal fiber with different diameters can be acquired by controlling the fiber-drawing speeds.

Figure 1(b) shows the radial concentration distribution of Cr^{3+} ions measured by laser scanning confocal microscopy (LSCM), which is calibrated by electron probe micro-analyzer (EPMA) [8]. The source rods used here were cut from YAG crystals, contained a mixture of 0.25 wt.% chromium (III) oxide (Cr_2O_3) and less than 0.1 wt% calcium (II) oxide (CaO) [9]. The LSCM sensitivity was 4.4×10^{-4} wt.% with 0.1-sec/pixel scan rate. The measurement using EPMA was the sensivity of 0.01 wt.% with a 240-sec-per-spot scan rate and cannot distinguish between the oxidation states of ions. By comparing Cr^{3+} and Cr^{4+} fluorescence, it shows most of the Cr ions are Cr^{3+} and the radial dopant profiles are able to reflect that of Cr_2O_3. Figure 1 (c) shows the normalized radial dopant profiles at the growth front in simulations which are consistent with that of grown crystal fibers in *ex-situ* measurements. It is noted that the shapes of growth front and air/melt interface, dominant by the allowable laser power and reduction ratio, rather than fluid flow determine the radial dopant profile.

Figure 2 (a)-(f) shows the dependence of the reduction ratios on the streamlines, normalized concentrations and isotherms. The Cr ions are getting denser from the growth to feed front while the reduction ratio decreases due to segregation effect and accumulated more near the feed front. The intervals of concentration contour lines are uniform and symmetric in 100-% case. The interval is getting narrower near the growth front and wider near the feed front for smaller reduction ratios because the interval is proportional to the dopant diffusion velocity due to the continuity. The inclination of dopant contour lines presents owing to the deformation of the air/melt interface when the reduction ratio or the allowable laser power decreases. The contour lines are always perpendicular to both air/melt interface and z axis defined by concentration boundary conditions without perturbation and vaporization at the air/melt interface. Compared to the bulk crystal growth [10], this assumption is closer to the real conditions for the much smaller air/melt surface area of miniature molten zone.

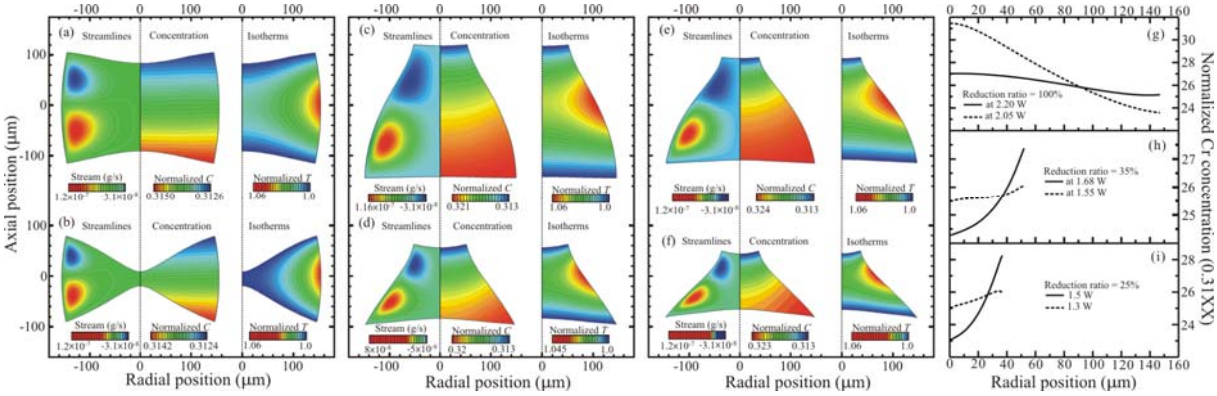

Figure 2. The streamlines (left), normalized Cr ion concentration (middle), and isotherms (right) in the miniature molten zones at the high and low allowable laser powers (top and bottom row) for the reduction ratios of (a)(b) 100%, (c)(d) 35%, and (e)(f) 25% while K=3.2 [11], $\partial\gamma/\partial T$ = -3.5×10^{-2} $dyn \cdot cm^{-1} \cdot K^{-1}$ [12] and D=10^{-2} $cm^2 \cdot s^{-1}$. The corresponding normalized radial dopant profiles at the growth front are for the reduction ratios of (g) 100%, (h) 35%, and (i) 25%.

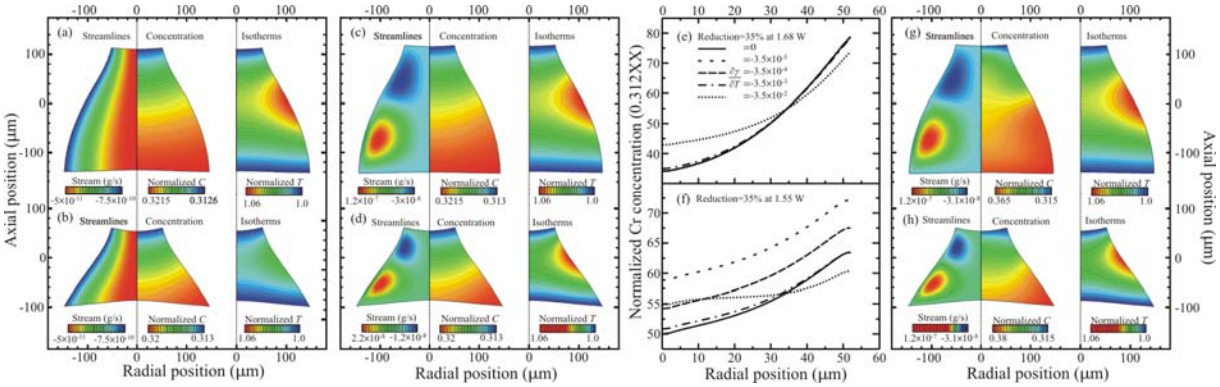

Figure 3. The streamlines (left), normalized Cr ions concentration (middle), and isotherms (right) in the miniature molten zones for the reduction ratios of 35% while K=3.2, D=10^{-2} $cm^2 \cdot s^{-1}$ and $\partial\gamma/\partial T$ = (a)(b) 0, (c)(d) -3.5×10^{-2} $dyn \cdot cm^{-1} \cdot K^{-1}$, and (g)(h) for D = 10^{-3} $cm^2 \cdot s^{-1}$ with $\partial\gamma/\partial T$ = -3.5×10^{-2} $dyn \cdot cm^{-1} \cdot K^{-1}$. (e)(f) The corresponding normalized radial dopant profiles at the growth front for various values of $\partial\gamma/\partial T$. Top and bottom rows are at high and low allowable laser powers of 1.68 W and 1.55 W, respectively

The corresponding normalized radial dopant profiles at the growth front in Fig. 2 (g)-(i) indicates that both the inclination of contour lines and the shapes of growth front determine the radial dopant profiles. The growth front and the air/melt interface becomes smooth and convex outward, respectively, from low to high allowable laser powers. A parabolic-like profile can be obtained for the non-unity reduction ratio. It is viable to adjust the air/melt interface, the distribution of mass or diffusion flow as well as reduction ratio, and especially the growth front to obtain a desirable radial dopant profile as well as that of refractive index for light guide or active devices.

Figure 3 (a)-(d) shows that the thermocapillary mass flow increases as $\partial\gamma/\partial T$ is increased. For pure YAG, the resulting magnitude of mass flow is on the order of 10^{-5}-10^{-4} $g \cdot s^{-1}$. The corresponding normalized radial dopant profiles at the growth front in Fig. 3 (e)(f) are steeper at 1.68 W because of the zone shape. It becomes smooth if the magnitude of $\partial\gamma/\partial T$ is higher than -3.5×10^{-3} $dyn \cdot cm^{-1} \cdot K^{-1}$ since the strong enough thermocapillary convection with clockwise upper eddy to collect the dopant ions from periphery to center near the growth front. The concentration level is shifted at various values of $\partial\gamma/\partial T$ because the influence of thermocapillary convection cannot be neglected at low allowable power or smaller volume of melt zone. Figure 3 (g)(h) shows that the thermocapillary convection compared to dopant diffusion velocity cannot be neglected and then affect the concentration distribution in the melt or the radial dopant profile of grown crystal fiber if the diffusion coefficient is smaller than the order of 10^{-3} $cm^2 \cdot s^{-1}$. The diffusion velocity of all Cr ions as much lighter solute is higher than that of mass flow in YAG streamlines as much heavier solvent. The weight ratio of these two particles is ~8.75%.

CONCLUSION

After the confirmation of the zone shapes and the further analysis of heat transfer and fluid flow, the governing equation and boundary condition of concentration are added here. The radial dopant profiles at the growth front verified by the *ex-situ* measurement are analyzed for high quality crystal-fiber devices. In macroscopic view, the level of average dopant concentration might be raised with a low enough $\partial\gamma/\partial T$ at the low allowable laser power, but a smoother profiles are obtained. Diffusion coefficient of Cr:YAG crystal should be higher than the order of 10^{-3} $cm^2 \cdot s^{-1}$ for the absence of the influence on the dopant distribution. The more precise quantitative comparison for other dopants in YAG, such as Nd:YAG crystal with K is 0.18 [10], can be investigated further by including the concentration of source rod as the initial value and the crystallization dynamics in microscopic view.

REFERENCES

[1] C. N. Tasi, Y. S. Lin, K. Y. Huang, Y. S. Lin, C. C. Lai, and S. L. Huang, Jpn. J. Appl. Phys., vol.47, pp.6369-6373, 2008.
[2] C. C. Lai, K.Y. Huang, H. J. Tasi, K. Y. Hsu, S. K. Liu, C. T. Cheng, K. D. Ji, C. P. Ke, S. R. Lin, and S. L. Huang, Opt. Lett., vol. 34, pp. 2357-2359, 2009.
[3] L. M. Lee, S. C. Pei, D. F. Lin, M. C. Tsai, T. M. Tai, P. C. Chiu, D. H. Sun, A. H. Kung, and S. L. Huang, J. Opt. Soc. Am. B, vol. 24, pp. 1909-1915, 2007.
[4] P. Y. Chen, C. L. Chang, K. Y. Huang, C. W. Lan, W. H. Cheng, and S. L. Huang, J. Appl. Crystallogr., vol. 42, pp.553-563, 2009.
[5] P. Y. Chen, C. L. Chang, K. Y. Huang, C. W. Lan, W. H. Cheng, and S. L. Huang, Jpn. J. Appl. Phys., vol. 48, pp. 115504, 2009.
[6] C. L. Chang, S. L. Huang, C. Y. Lo, C. W. Lan, W. H. Cheng, and P. Y. Chen, accepted by J. Cryst. Growth, 2010.
[7] C. W. Lan and S. Kou, J. Cryst. Growth, vol.132, pp.578-591, 1993.
[8] V. J. Fratello and C. D. Brandle, J. Cryst. Growth, vol.128, pp.1006-1010, 1993.
[9] S. Ishibashi, K. Naganuma and I. Yokohama, J. Cryst. Growth, vol.183, pp.614-621, 1998.
[10] C. W. Lan and S. Kou, J. Cryst. Growth, vol. 108, pp.351-366, 1991.
[11] B. Henderson and Ralph H. Bartram, *Crystal-field engineering of solid-state laser material*, Cambridge University Press, 83-85 (2000).
[12] J. C. Chen, C. Y. Lo, K. Y. Huang, F. J. kao, S. Y. Tu and S. L. Huang, J. Cryst. Growth, vol. 274, pp.522-529, 2005.